Supporting Information

Electronic modulation of cobalt-molybdenum oxide via Te doping embedded in carbon matrix for superior overall water splitting

Luqi Wang[a], Hanzhi Yu[a], Sheng Zhao[a], Hui Ma[b], Linlin Li*[a], Feng Hu[a], Lei Li*[b], Hui Pan[c], K. M. El-Khatib[d] and Shengjie Peng*[a]

[a]College of Materials Science and Technology, Nanjing University of Aeronautics and Astronautics, Nanjing 210016, China. E-mails: lilinlin@nuaa.edu.cn pengshengjie@nuaa.edu.cn
[b]College of Biological, Chemical Sciences and Engineering, Jiaxing University, 118 Jiahang Road, Jiaxing, Zhejiang, 314001, PR China.
E-mail: leili@mail.zjxu.edu.cn
[c]Institute of Applied Physics and Materials Engineering, University of Macau, Avenida da Universidade, Taipa, Macao 999078, P. R. China
[d]Chemical Engineering and Pilot Plant Department, Engineering Research Institute
National Research Centre 33 El-Buhouth St., Dokki, Cairo 12622, Egypt

TOF calculation

Turnover frequency (TOF) was calculated via the following formula according to previous reports.

$$\text{TOF per site} = \frac{\#\ \text{Total Oxygen Turn Over/cm}^2\ \text{geometric area}}{\#\ \text{Surface Sites/cm}^2\ \text{geometric area}}$$

The total number of oxygens turnovers was calculated from the current density using the following equation:

$$\#O_2 = \left(j\frac{\text{mA}}{\text{cm}^2}\right)\left(\frac{1\text{C s}^{-1}}{1000\text{ mA}}\right)\left(\frac{1\text{ mol s}^{-1}}{1000\text{ mA}}\right)\left(\frac{1\text{ mol O}_2}{4\text{ mol e}^-}\right)\left(\frac{6.022\times10^{23}\text{O}_2\text{ molecules}}{1\text{ mol O}_2}\right) = J\times1.56\times10^{15}\frac{\text{O}_2/\text{s}}{\text{cm}^2}\text{per}\frac{\text{mA}}{\text{cm}^2}$$

The Co content of Te-$CoMoO_3$@C is determined by the ICP. The mass loading on the electrode is ~0.30 mg cm^{-2}. Thus, n is calculated as:

$$n(\text{Te–CoMoO}_3\text{@C}) = \frac{4.67\%\times0.30\frac{\text{mg}}{\text{cm}^2}}{58.93\frac{\text{g}}{\text{mol}}} = 2.38\times10^{-7}\text{ mol/cm}^2$$

$$N^{\text{Te - CoMoO}_3\text{@C}}_{\text{active}} = 6.022\times10^{23}\text{mol}^{-1}\times2.38\times10^{-7}\text{mol/cm}^2 = 1.433\times10^{17}\text{ atoms/cm}^2$$

$$\mathrm{TOF} = \frac{|J| \times 1.56 \times 10^{15} \frac{O_2/s}{cm^2} \mathrm{per} \frac{mA}{cm^2}}{N_{active}^{Te-CoMoO_3@C}}$$

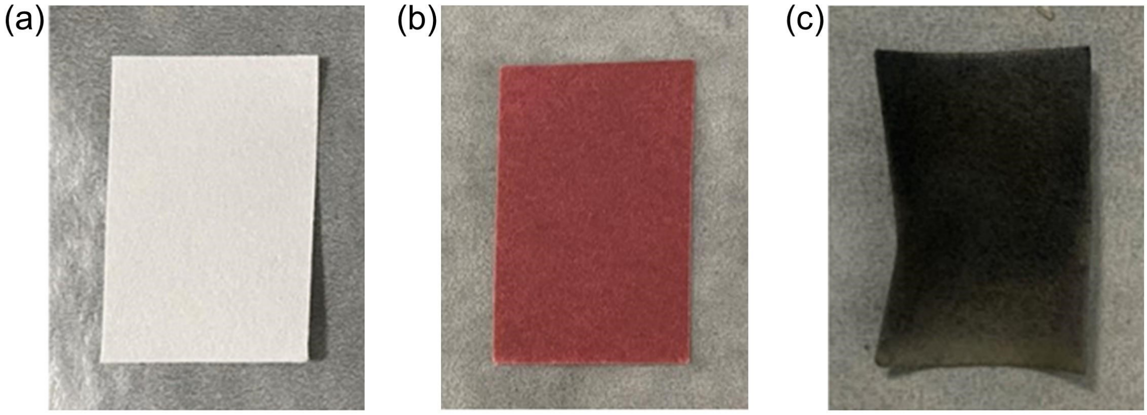

Fig. S1. Optical photographs of (a) filter paper, (b) Co/Mo salts adsorbed on the filter paper, and (c) Te-$CoMoO_3$@C.

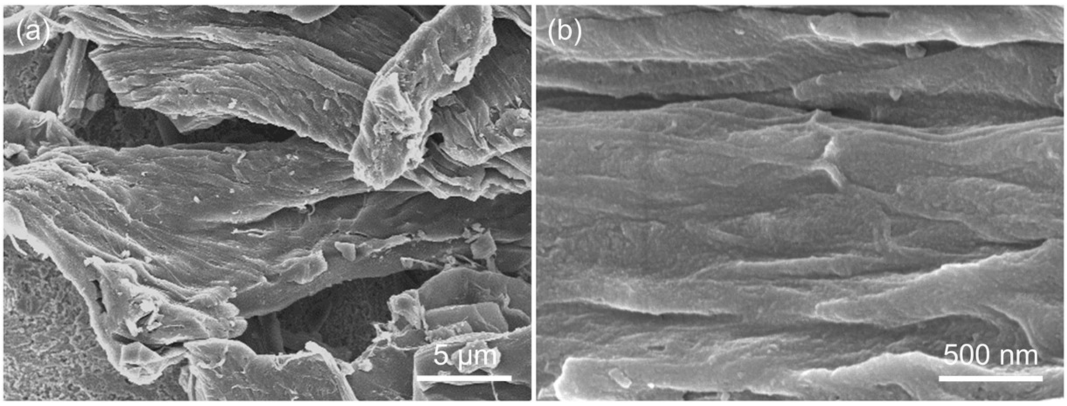

Fig. S2. (a) Low-magnified and (b) high-magnified SEM images of calcined filter paper.

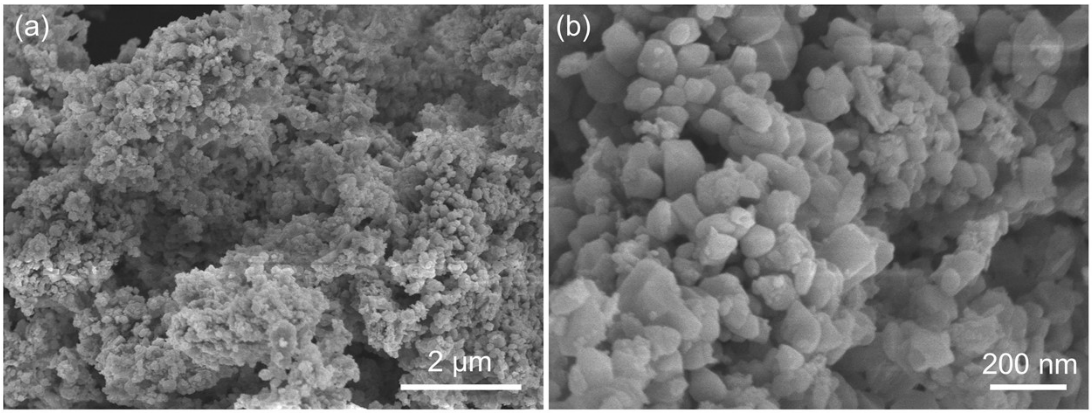

Fig. S3. (a) Low-magnified and (b) high-magnified SEM images of $CoMoO_3$@C.

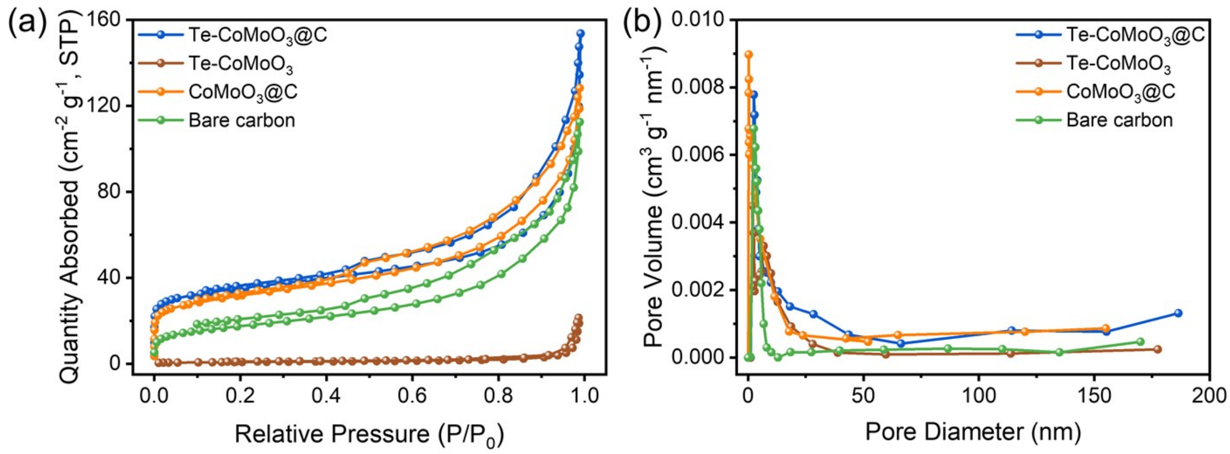

Fig. S4. (a) N_2 adsorption/desorption isotherm and (b) the corresponding pore size distribution of Te-$CoMoO_3$@C, Te-$CoMoO_3$, $CoMoO_3$@C, and bare carbon.

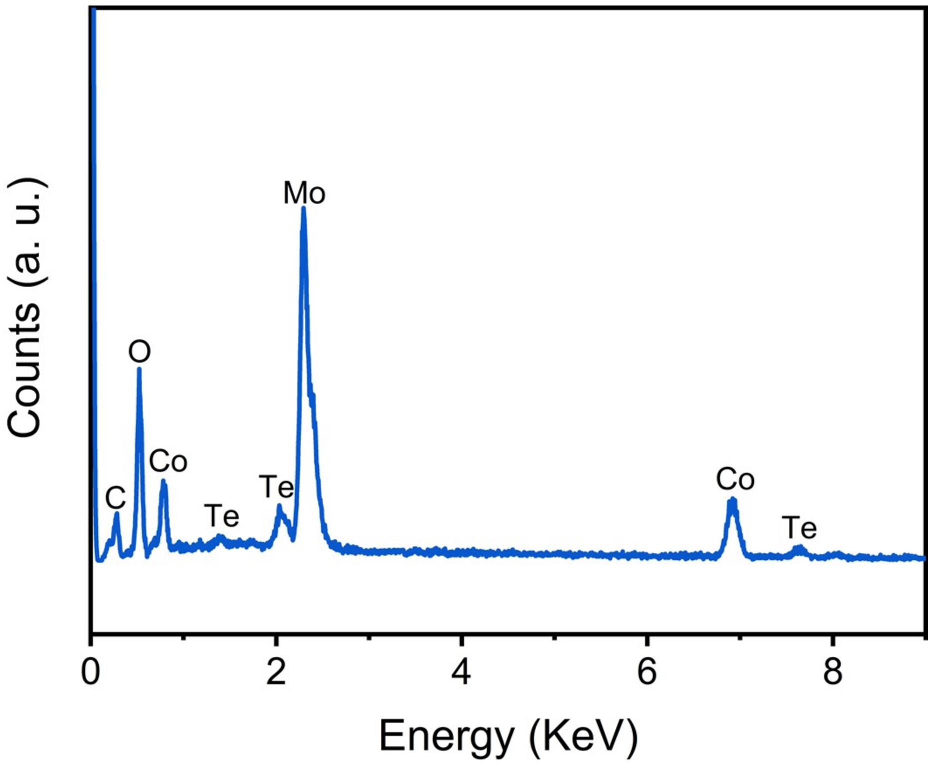

Fig. S5. EDX pattern of Te-$CoMoO_3$@C.

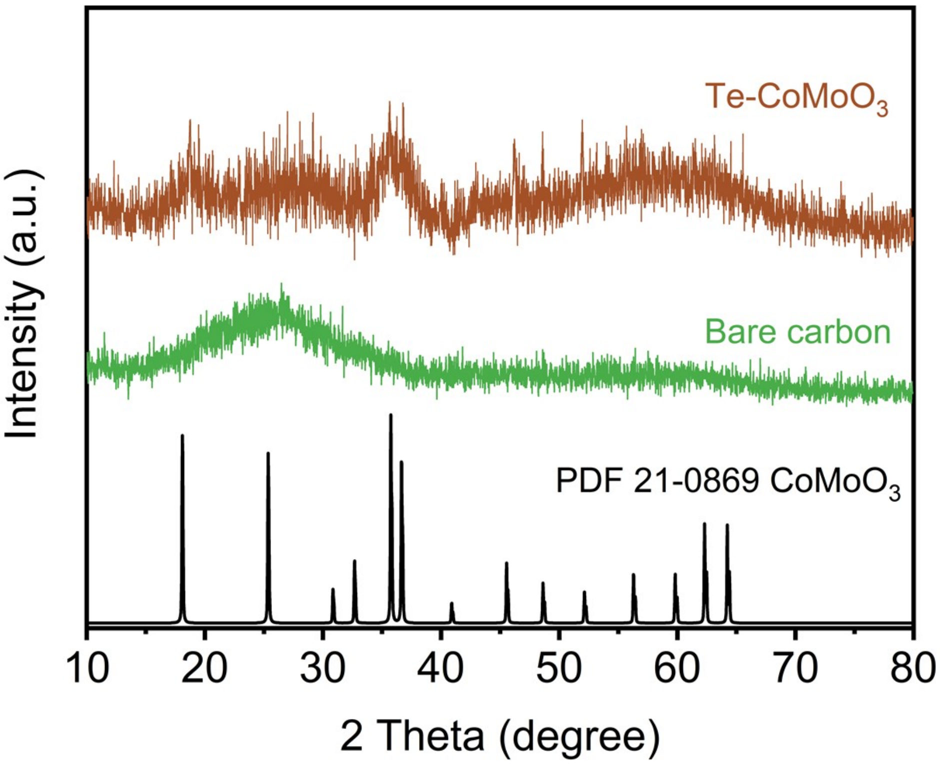

Fig. S6. XRD pattern of $CoMoO_3$@C and bare carbon.

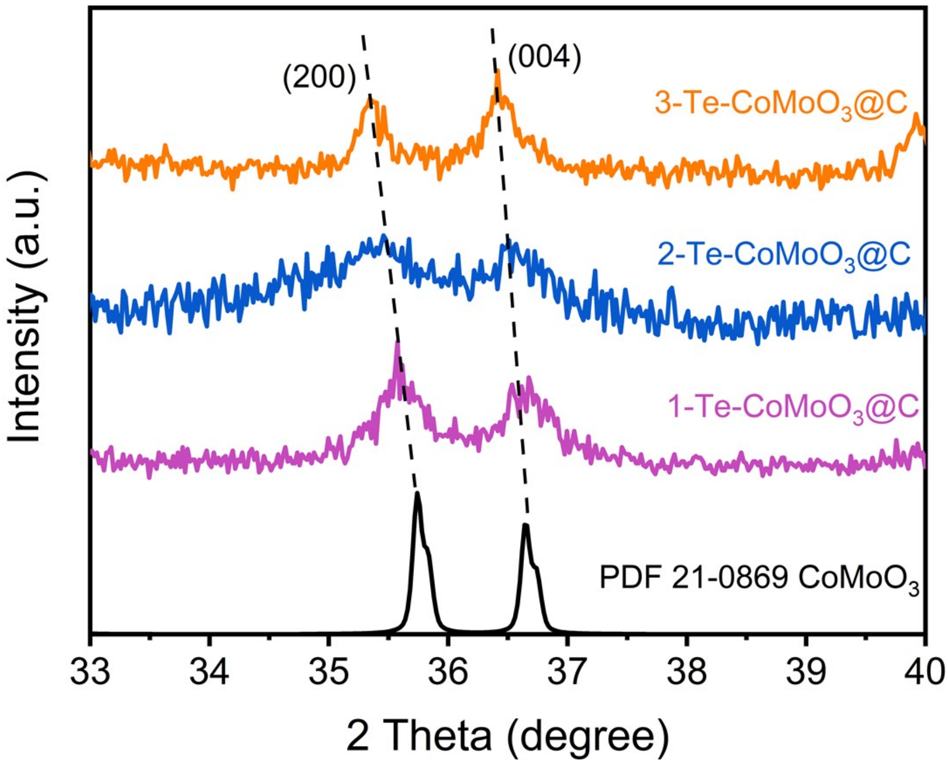

Fig. S7. XRD patterns of the Te-$CoMoO_3$@C with various doping amounts of Te.

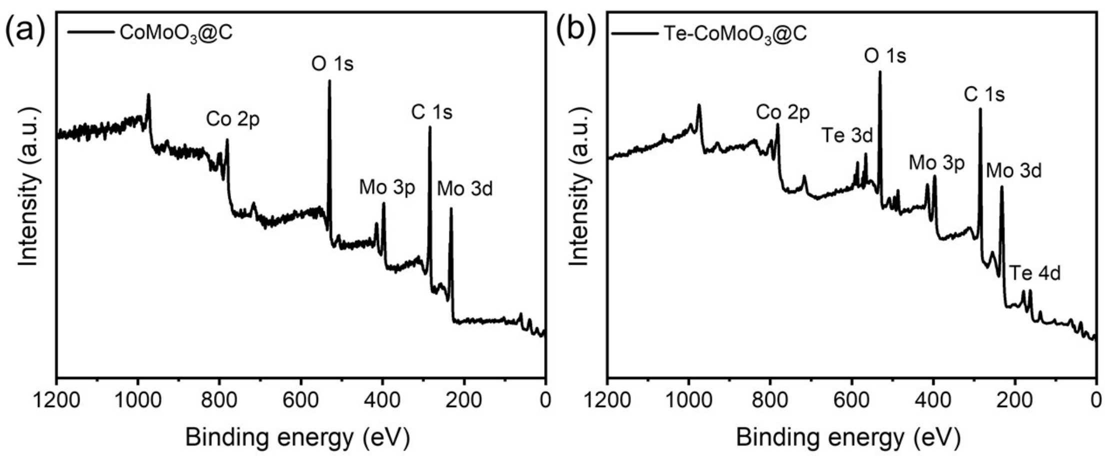

Fig. S8. XPS full spectra of (a) $CoMoO_3$@C and (b) Te-$CoMoO_3$@C.

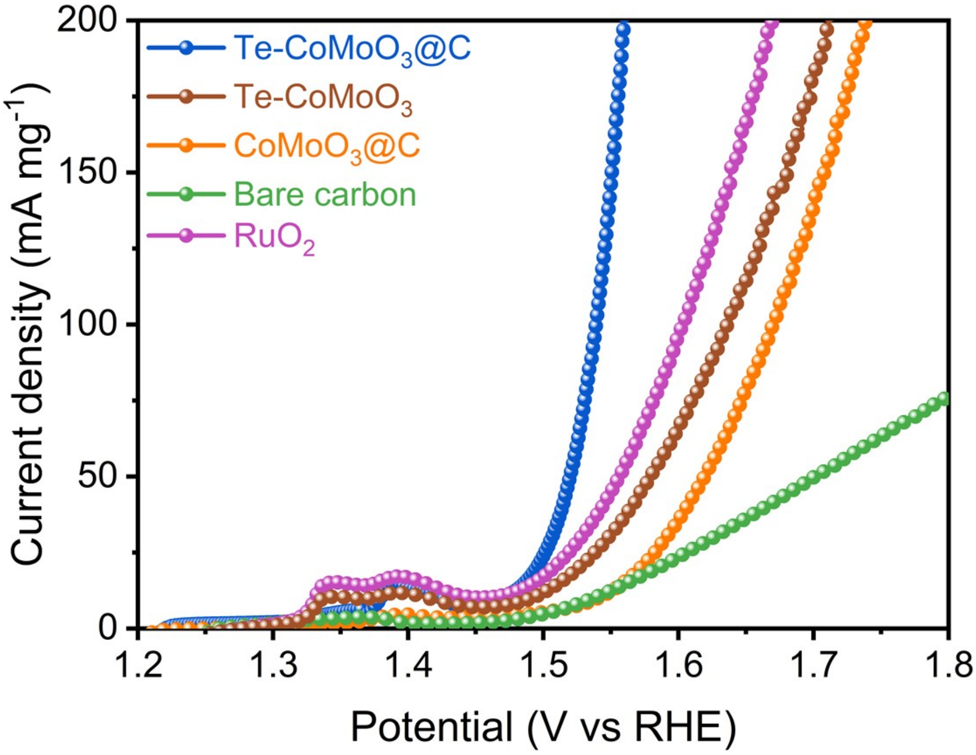

Fig. S9. OER LSV polarization curves normalized to catalyst loading of RuO_2, bare carbon, $CoMoO_3$@C, Te-$CoMoO_3$ and Te-$CoMoO_3$@C.

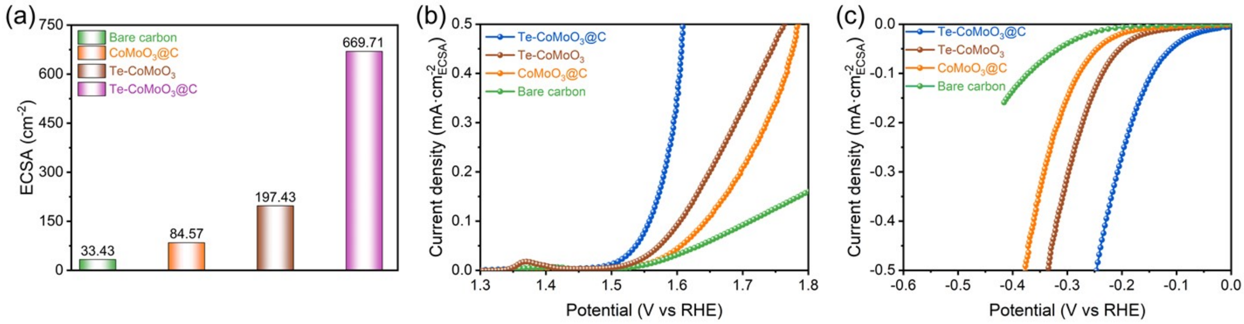

Fig. S10. (a) The ECSA of bare carbon, $CoMoO_3$@C, Te-$CoMoO_3$ and Te-$CoMoO_3$@C. (b) HER and (c) OER polarization curve normalized by the ECSA for bare carbon, $CoMoO_3$@C, Te-$CoMoO_3$ and Te-$CoMoO_3$@C.

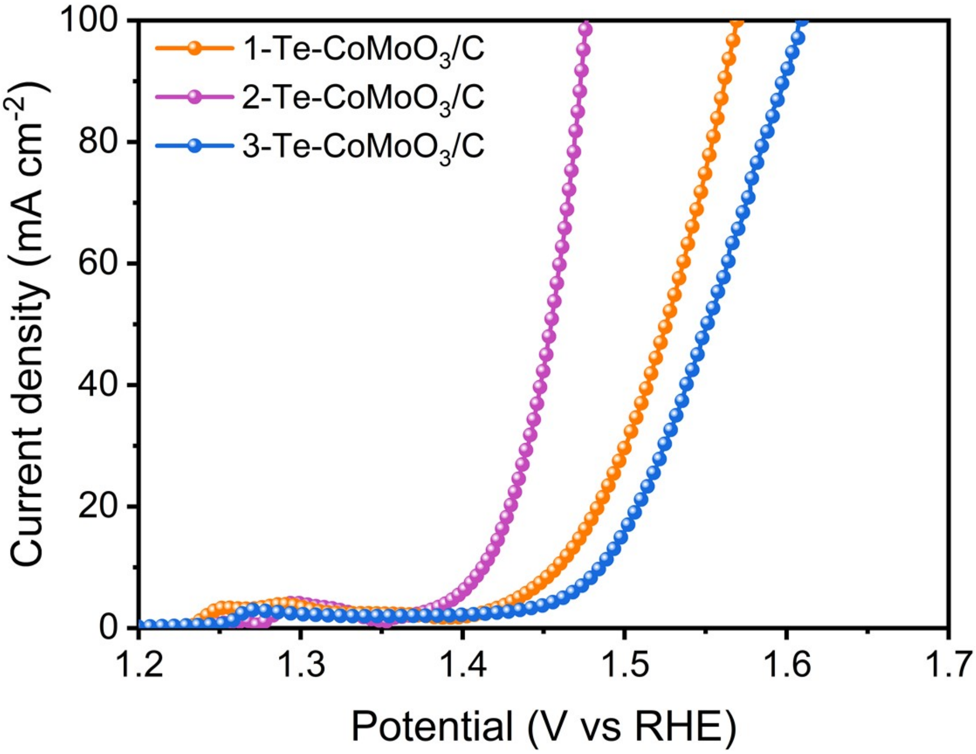

Fig. S11. OER performances of 1-Te-$CoMoO_3$@C, 2-Te-$CoMoO_3$@C, and 3-Te-$CoMoO_3$@C.

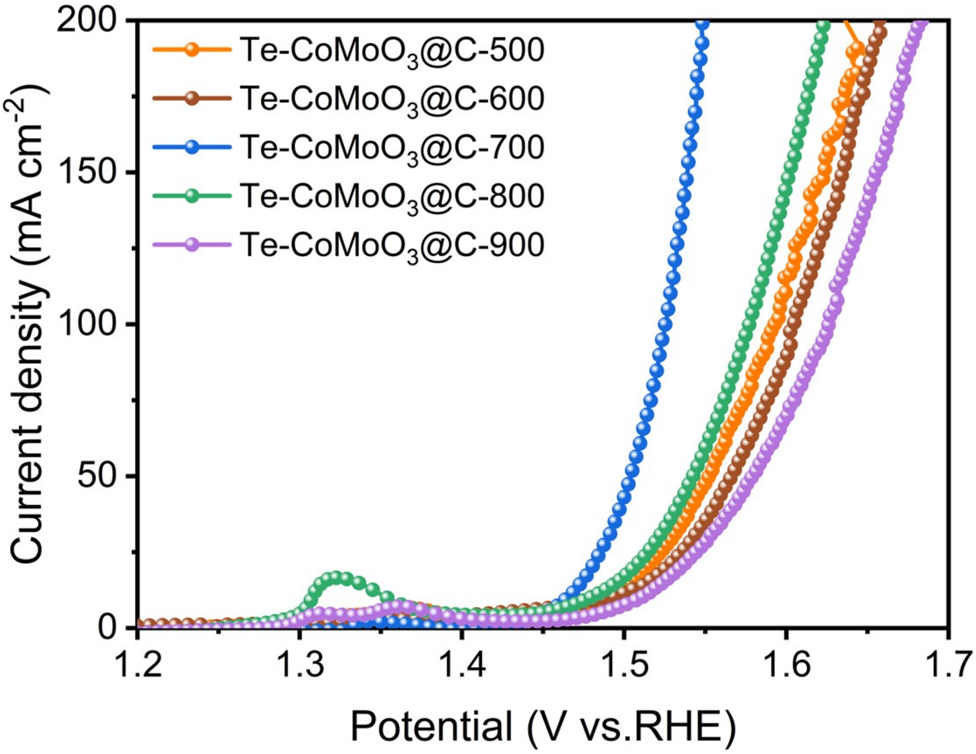

Fig. S12. OER performances of Te-$CoMoO_3$@C catalysts obtained under different temperatures.

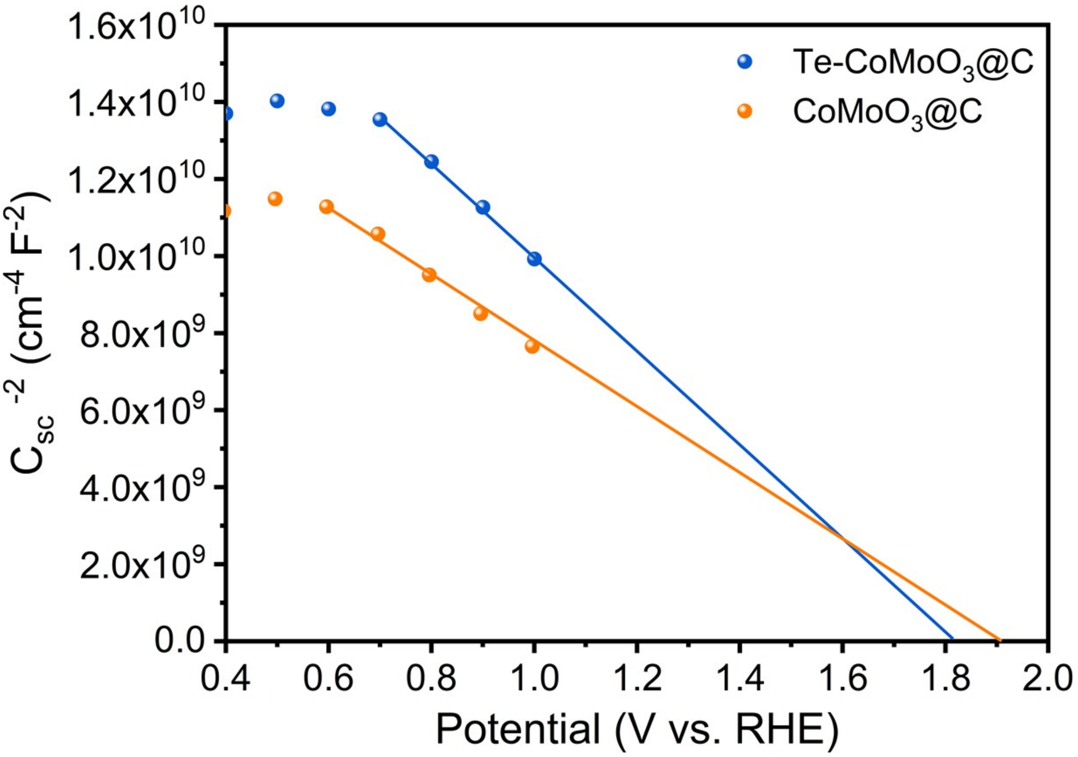

Fig. S13. Mott-Schottky curves of $CoMoO_3@C$ and Te-$CoMoO_3@C$.

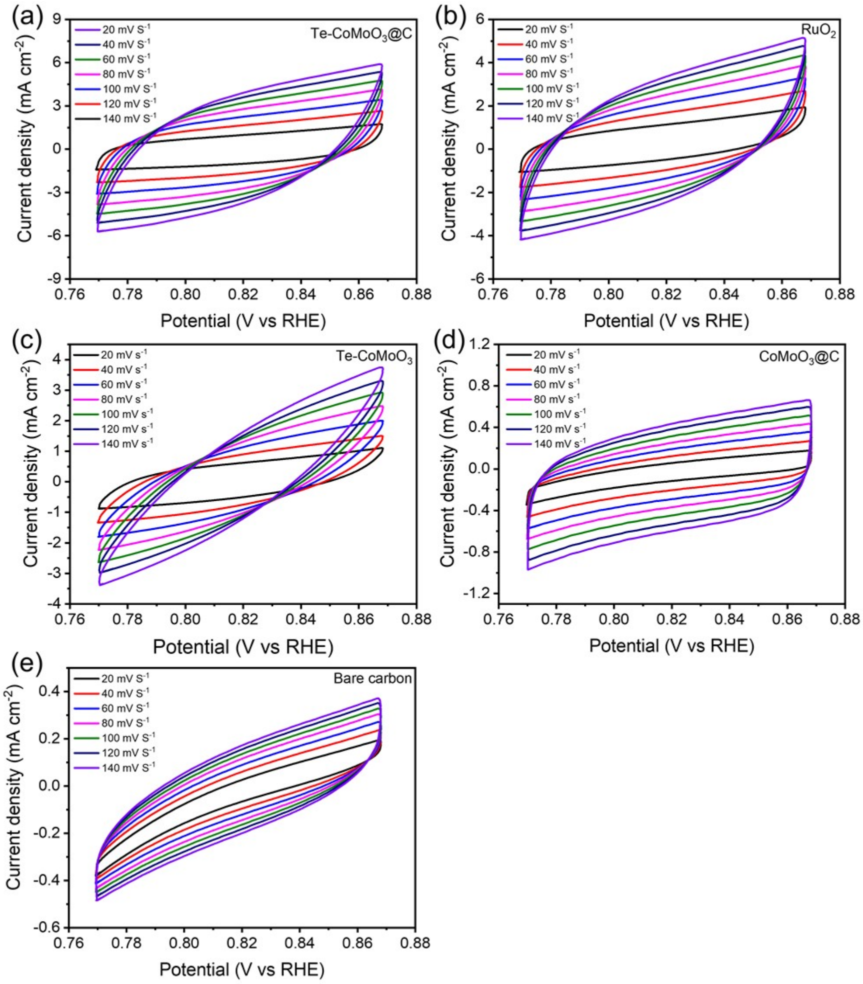

Fig. S14. Cyclic voltammograms of different samples from 20 to 140 mV s^{-1} between 0.77 and 0.87 V.

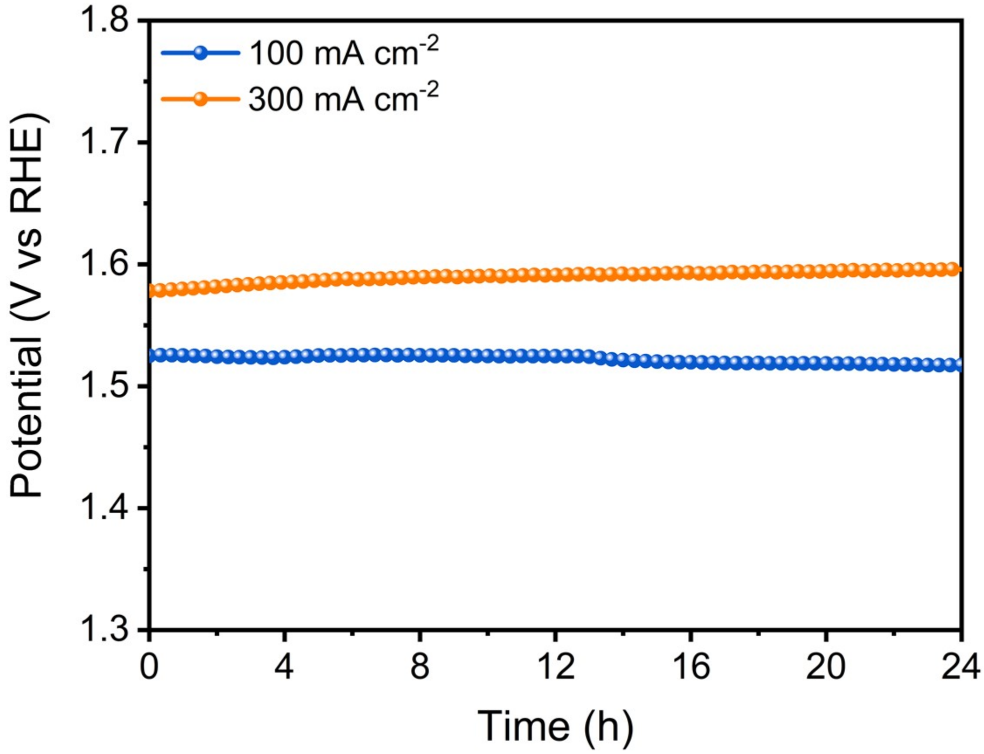

Fig. S15. Chronopotentiometry curves of Te-$CoMoO_3$@C during OER process.

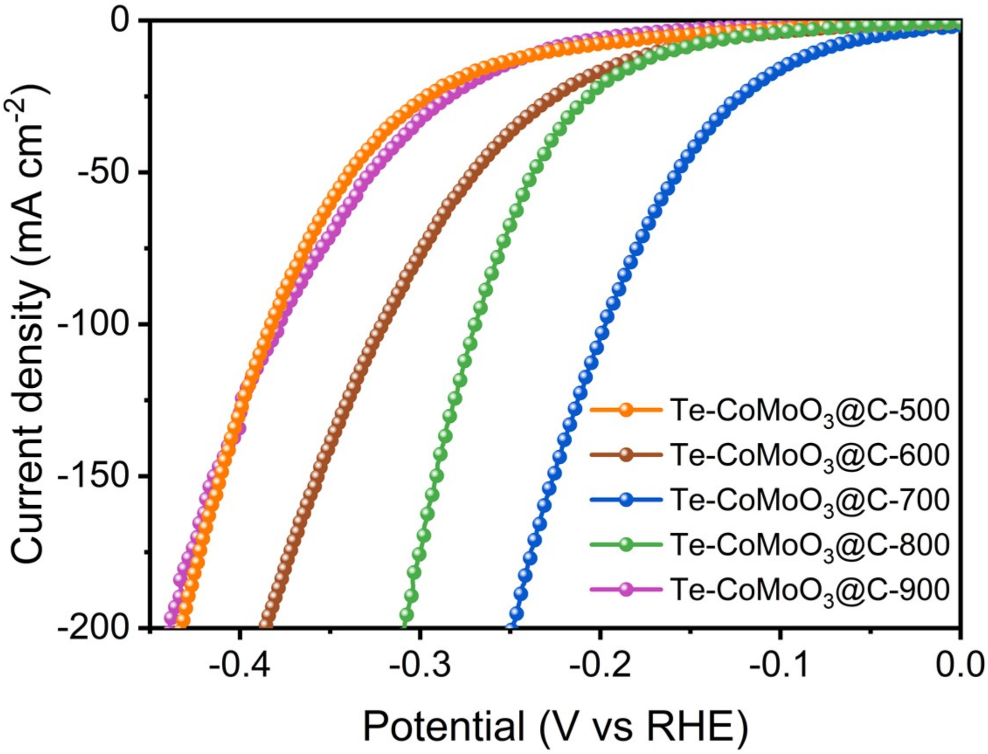

Fig. S16. HER performances of Te-$CoMoO_3$@C catalysts obtained under different temperatures.

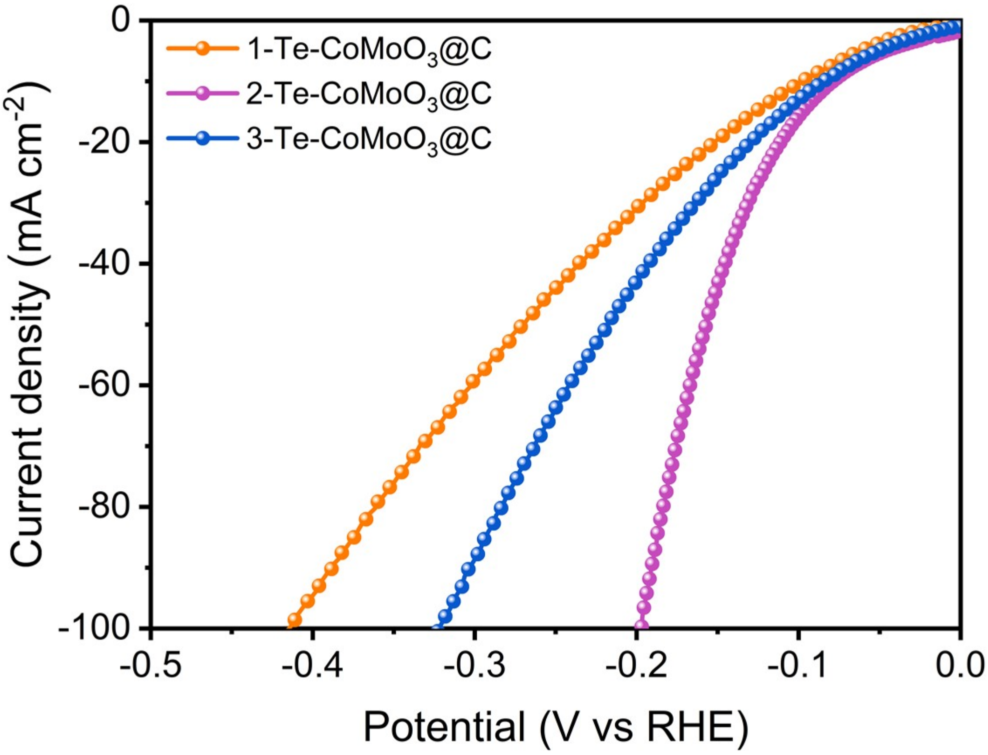

Fig. S17. HER performances of 1-Te-$CoMoO_3$@C, 2-Te-$CoMoO_3$@C, and 3-Te-$CoMoO_3$@C.

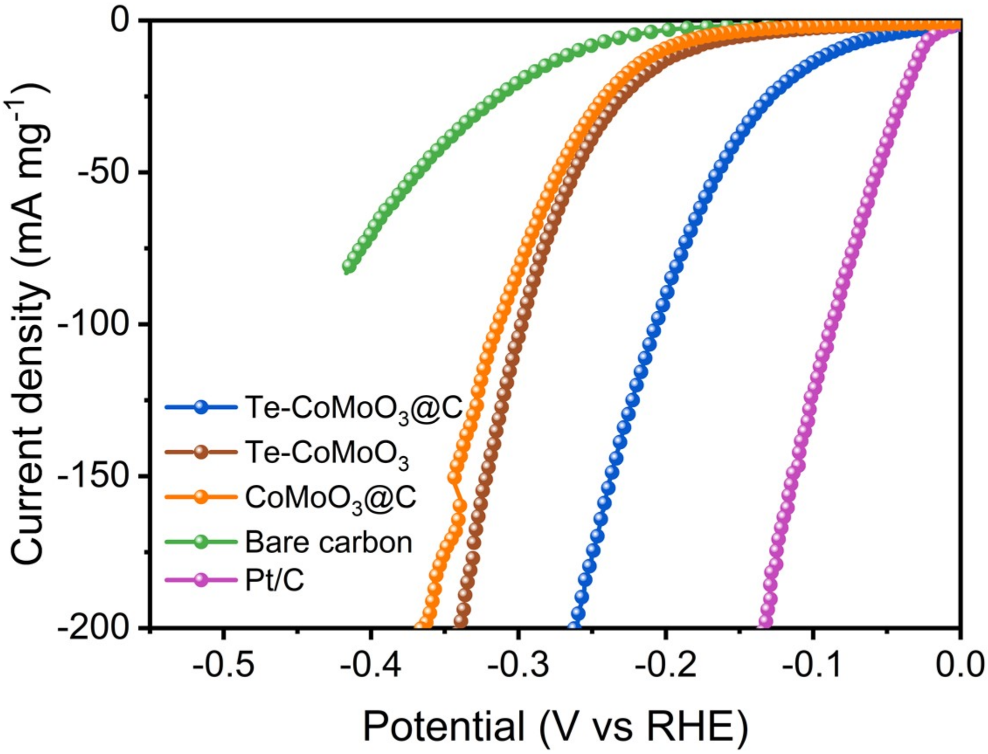

Fig. S18. HER LSV polarization curves normalized to catalyst loading of Pt/C, bare carbon, $CoMoO_3$@C, Te-$CoMoO_3$ and Te-$CoMoO_3$@C.

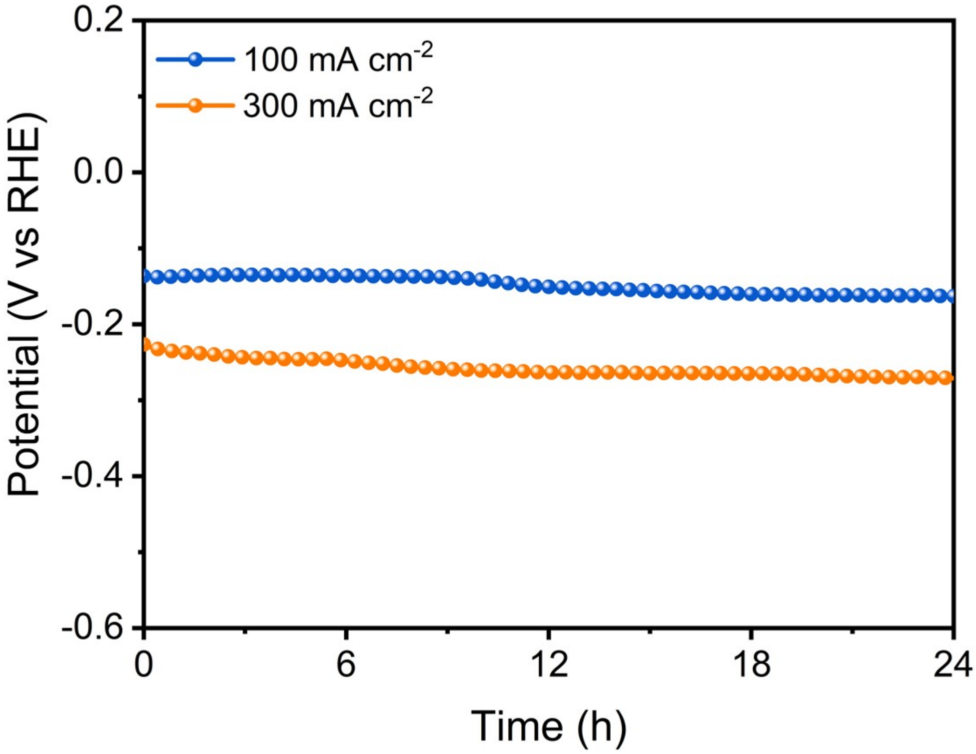

Fig. S19. Chronopotentiometry curves of Te-$CoMoO_3$@C during HER process.

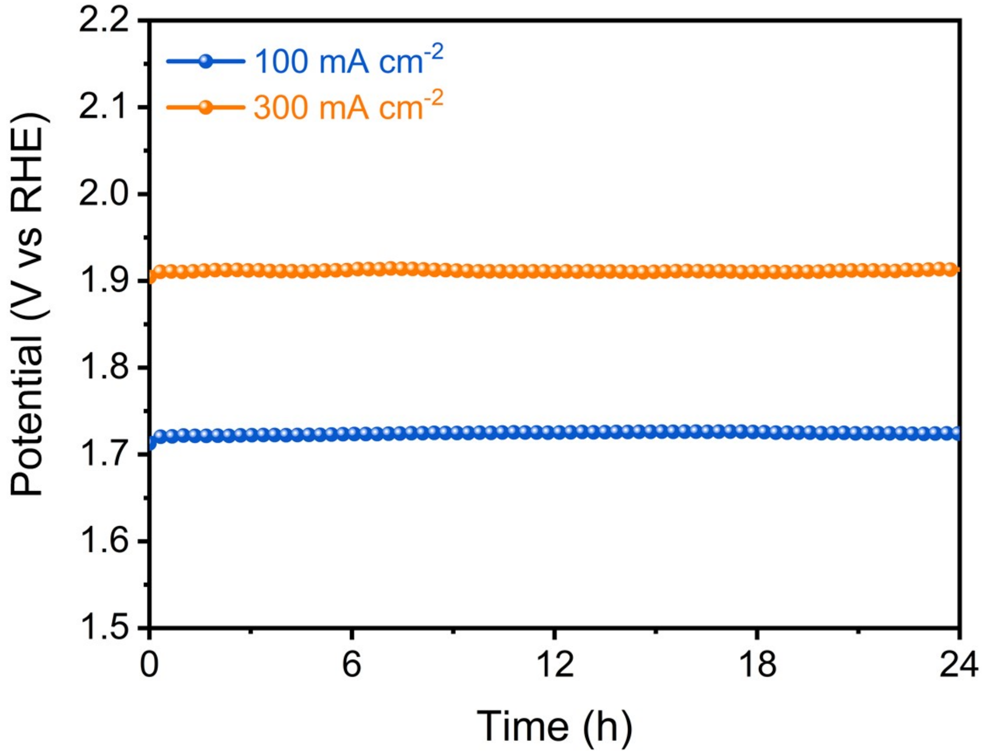

Fig. S20. Chronopotentiometry curves of Te-$CoMoO_3$@C during overall water splitting process.

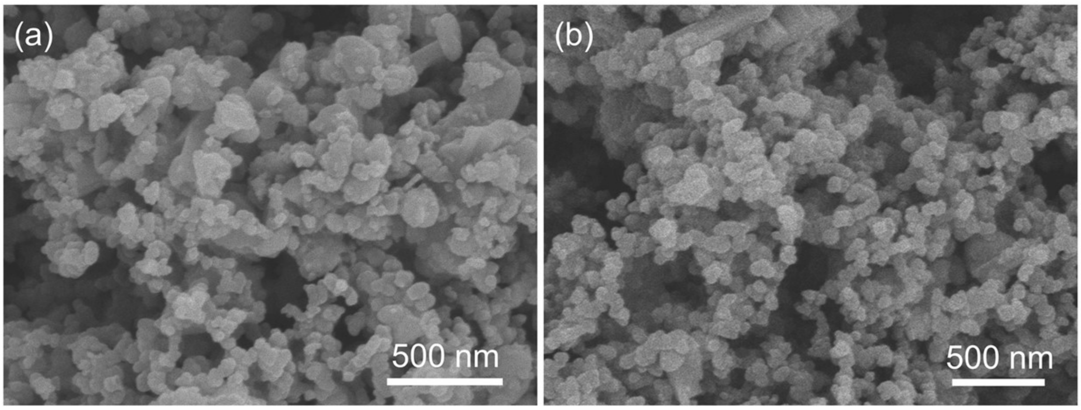

Fig. S21. SEM images of Te-$CoMoO_3$@C after OER (a) and (b) HER cycling tests.

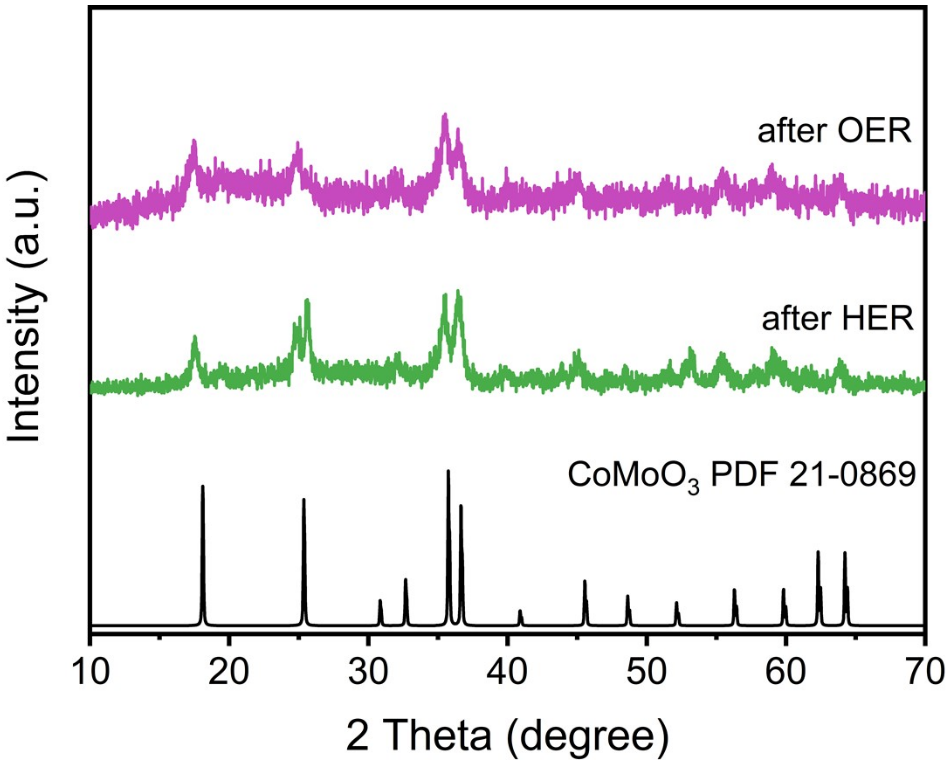

Fig. S22. XRD patterns of Te-$CoMoO_3$@C after water splitting cycling tests.

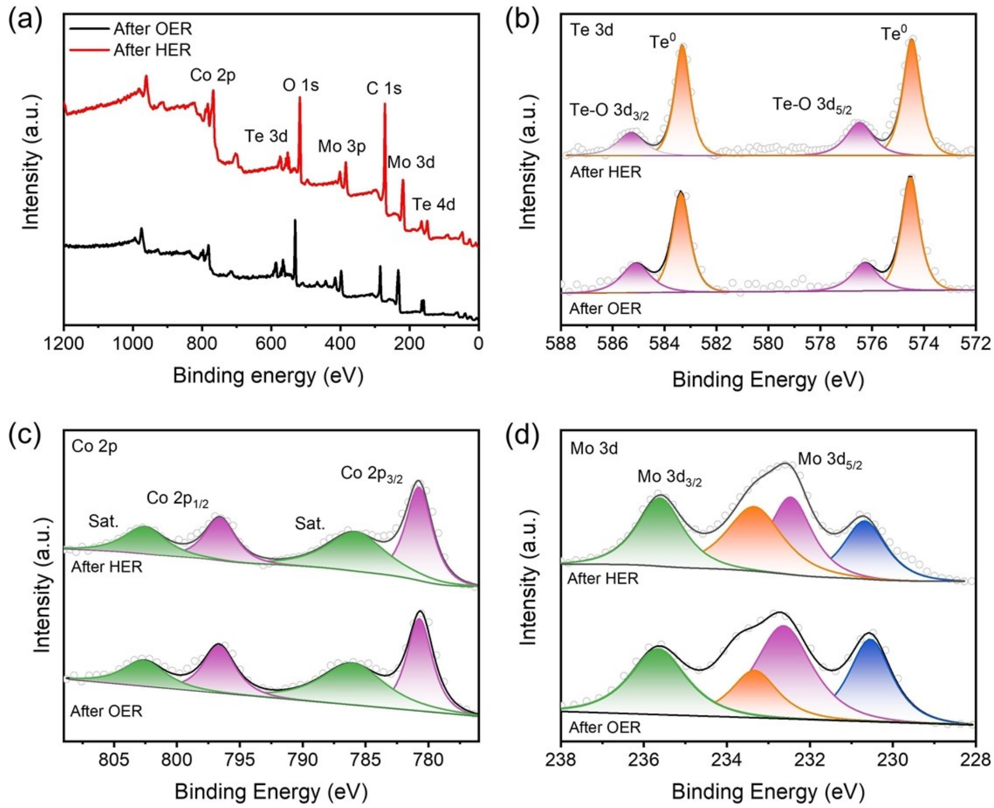

Fig. S23. (a) XPS survey spectra and high-resolution XPS spectra of (b) Te 3d, (c) Co 2p, and (d) Mo 3d for Te-$CoMoO_3$@C after water splitting cycling tests.

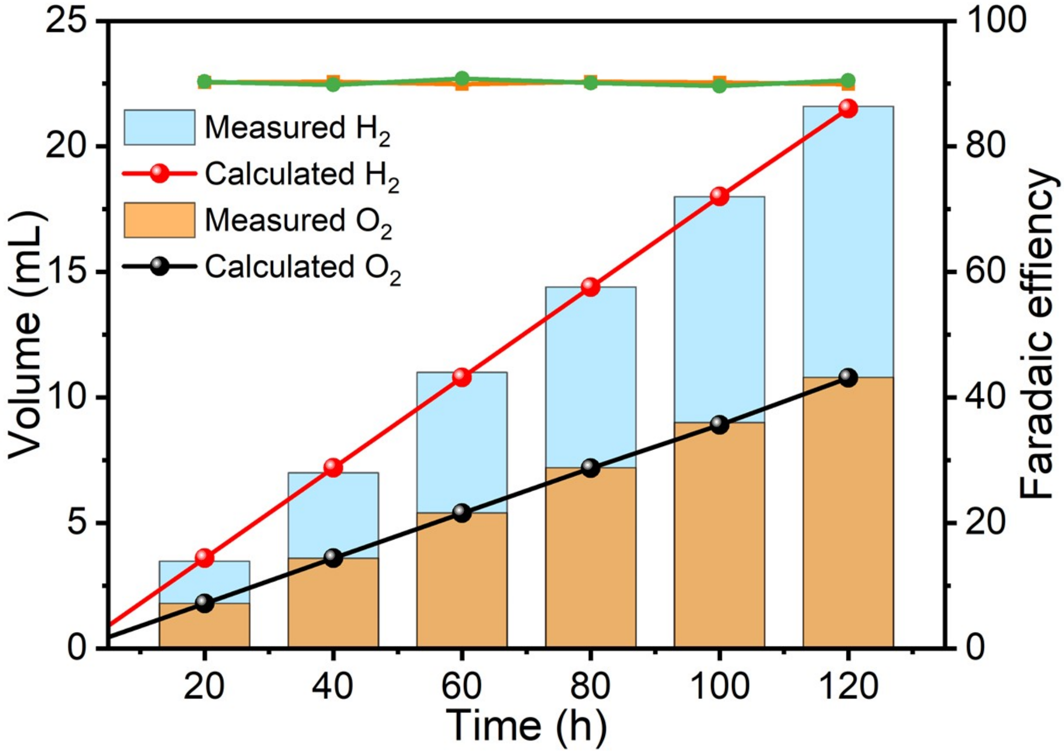

Fig. S24. Amount of hydrogen theoretically calculated and experimentally measured and the Faradaic efficiency.

Table S1. Inductive Coupled Plasma (ICP) results of prepared samples.

Samples	Te (wt.%)	Co (wt.%)	Mo (wt.%)
Te-$CoMoO_3$@C	0.83	4.67	18.32

Table S2. The fitting parameters of the XPS spectra of O2p for Te-$CoMoO_3$@C and $CoMoO_3$@C.

Sample	Peak	Position	peak area
Te-$CoMoO_3$@C	M-O	530.42	11705.17
	O_v	531.13	6338.04
	H-O-H	532.84	5005.15
$CoMoO_3$@C	M-O	530.51	51536.50
	O_v	531.25	3896.50
	H-O-H	532.77	16536.50

Table S3. OER Fitting results of EIS for Te-$CoMoO_3$/C, Te-$CoMoO_3$, $CoMoO_3$/C, bare carbon, and RuO_2.

Catalysts	Rs (ohm)	Rct (ohm)	Error (%)
Te-$CoMoO_3$@C	1.181	3.042	0.692
Te-$CoMoO_3$	1.326	4.683	0.688
$CoMoO_3$@C	1.558	6.919	0.795
Bare carbon	1.841	13.59	0.764
RuO_2	1.294	3.545	0.748

Table S4. Comparison of overpotential (10 mA cm^{-2}) and Tafel slopes for OER between Te-$CoMoO_3$@C and various reported catalysts.

Catalysts	Overpotential (mV) 10 mA cm^{-2}	Tafel slope (mV dec^{-1})	Reference
Te-$CoMoO_3$@C	**218**	**39**	**This work**
Te/FeNiOOH-NC	220	52	ACS Appl. Mater. Interfaces. 2021, 13, 10972-10978.
GB-$(Fe_{0.66}Co_{0.34})_2B$/RGO	221	39	Appl. Catal. B Environ. 2020, 305, 121034.
Ta-NiFe LDH	228	58.95	Chem. Eng. J. 2021, 403, 126297.
$Co_{1.6}Ni_{0.4}P_4O_{12}$-C	230	51.1	Adv. Funct. Mater. 2020, 30, 1910498.
Ni-MnO_2	233	36	Adv. Energy Mater. 2020, 10, 2001059.
V-NiCoP	234	35	J. Mater. Chem. A. 2021, 9, 12203-12213.
$Fe_{0.9}Ni_{2.1}S_2$@NF	235	64	Adv. Energy Mater. 2020, 10, 2001963.
Ni-Mo-P	235	108.4	Appl. Catal. B Environ. 2021, 298,

			120494.
Mo-Ni_3S_2/Ni_xP_y	236	60.6	Adv. Energy Mater. 2020, 10, 1903891.
S-NiFe-LDH-9-A	240	42	Appl. Catal. B Environ. 2021, 292, 120150.
o-$CoTe_2$|P@HPC/CNTs	241	46	ACS Nano. 2020, 14, 6968-6979.
Fe, Ni-CoS_2	242	35	ACS Catal. 2022, 12, 3743-3751.
30%Ce-NiFe-LDH	242	32	Energy Environ. Sci. 2020, 13, 2949-2956.
Ti-CoS_x HSS	249	48.3	Small. 2022, 18, 2103106.
CoOOH-W_D-Co_V	251	46.1	Adv. Mater. 2022, 34, 2104667.
$Fe_xNi_{3-x}S_2$@NF	252	64	Adv. Energy Mater. 2020, 10, 2001963.
NiNCs-1T-Mn-VTe_2 NS	258	65.11	Appl. Catal. B Environ. 2022, 301, 120780.
0.5Fe-$NiCo_2O_4$@CC	258	63.5	Small. 2022, 18, 2106187.
Co, Nb-MoS_2/TiO_2HSs	260	65	Nano Energy. 2021, 82, 105750.
Fe-Co_3O_4 HHNPs	262	43	Adv. Mater. 2020, 32, 2002235.
$Fe_{0.4}Co_{0.6}Se_2$	270	36	Energy Environ. Sci. 2021, 14, 365-373.
N-CoS_2 SSs	278	56	Adv. Sci. 2020, 7, 2001178.
Fe-NiSe NSs/CNTs	282	61	J. Mater. Chem. A. 2022, 10, 3102-3111.
P-Co_3O_4	283	85.3	Adv. Energy Mater. 2021, 11, 2100358.
$Co_2Mo_3O_8$	290	87.5	Angew. Chem. Int. Ed. 2020, 59, 11948-11957.
W-NiCoP/NF	295	99	Appl. Mater. Today. 2021, 24, 101154.
Fe-Mo/Te-2	300	45.6	Chem. Eng. J. 2021, 423, 130168.
Te-Co_3O_4	313	75	Int. J. Energy Res. 2021, 10, 1-10.

Table S5. HER fitting results of EIS for Te-$CoMoO_3$@C, Te-$CoMoO_3$, $CoMoO_3$@C, bare carbon, and Pt/C.

Catalysts	Rs (ohm)	Rct (ohm)	Error (%)
Te-$CoMoO_3$@C	1.264	5.162	0.609
Te-$CoMoO_3$	1.402	6.532	0.701
$CoMoO_3$@C	1.573	7.215	0.651
Bare carbon	1.728	11.36	0.770
Pt/C	1.153	3.531	0.686

Table S6. The comparison of water splitting performances of Te-$CoMoO_3$@C and other catalysts in the literature.

Catalysts	Overpotential (mV) 10 mA cm^{-2}	Stability (h)	Reference
Te-$CoMoO_3$@C	**1.54**	**100**	**This work**
DV-MnO_2	1.55	100	Adv. Funct. Mater. 2021, 31, 2010718.
Fe-Ni_5P_4/NiFeOH-350	1.55	20	Appl. Catal. B Environ. 2021, 291, 119987.
V-NiCoP	1.56	56	J. Mater. Chem. A. 2021, 9, 12203-12213.
WN-Ni@ N, P-CNT-800	1.57	10	Appl. Catal. B Environ. 2021, 298, 120511.
Fe-doped NiSe NSs/CNTs	1.57	24	J. Mater. Chem. A. 2022, 10, 3102-3111.
Co, Nb-MoS_2/TiO_2HSs	1.57	60	Nano Energy. 2021, 82, 105750.
E-Mo-NiCoP-3	1.58	48	Nano-Micro Letters. 2019, 11, 55.
P-Co_3O_4	1.6	60	Adv. Energy Mater. 2021, 11, 2100358.
Ni-Fe-$K_{0.23}$ MnO_2 CNFs-300	1.62	24	Small. 2020, 16, 1905223.
Mn-CoP@ Mn-CoOOH	1.64	24	Appl. Catal. B Environ. 2021, 292, 120172.

Table S7. Overall water splitting fitting results of EIS for Te-$CoMoO_3$@C, Te-$CoMoO_3$, $CoMoO_3$@C, bare carbon, and Pt/C||RuO_2.

Catalysts	Rs (ohm)	Rct (ohm)	Error (%)
Te-$CoMoO_3$@C	1.035	2.435	0.863
Te-$CoMoO_3$	1.468	8.536	1.328
$CoMoO_3$@C	1.657	10.368	1.143
Bare carbon	1.983	14.723	0.953
Pt/C||RuO_2	1.172	3.879	1.035